

# NUMERICAL SIMULATION OF THE VISCOUS FLOW AROUND SHIPS TURNING IN SHALLOW WATER

Reference NO. IJME 1242, DOI: 10.5750/ijme.v164iA3.1242

**H M Wang, X Y Chen, H M Yu**, School of Naval Architecture and Maritime, Zhejiang Ocean University, China, **L Chen\***, Donghai Science and Technology College, Zhejiang Ocean University, China, **T Wang, J R Xu**, School of Marine Engineering Equipment, Zhejiang Ocean University, China, and **X F Wang**, Shanghai Zhenhua Heavy Industries Company Limited, China.

KEY DATES: Submitted: 04/02/21; Final acceptance: 10/10/22; Published: 31/01/23

\*Corresponding author: chenlinhm@126.com (L Chen)

## SUMMARY

Due to the effect of water depth, hydrodynamic characteristics of ships manoeuvring in shallow waters are quite different from those in deep water. In the present study, the CFD method is used to investigate the hydrodynamic behaviour of the ESSO OSAKA model in model-fixed condition in deep and shallow waters by solving RANS equations, which performs steady turning motion with the effect of free surface considered. The governing equations are discretized by the finite volume method (FVM) and the free surface is captured by applying the volume of fluid (VOF) method. Viscous hydrodynamic characteristics and flow fields in a series of cases at different water depths and speeds are investigated respectively. By comparing the numerical results in shallow water with those in deep water, it was found that effects of water depth and free surface are significant on ship's hydrodynamic forces. The coefficients of drag, lateral force and yaw moment all increase with the decrease of water depth. The drag coefficient in shallow water is about 45% larger than that in deep water. However, effect of water depth on the lateral force coefficient is small, it is about 15% larger in shallow water than that in deep water. While, it has significant effect on the yaw moment coefficient, which is about 25% larger in shallow water than in deep water. And as the water depth increases, the effect of the free surface gradually becomes smaller. Both coefficient of pressure component of drag force and drag coefficient in the present simulation are about 7% smaller than the case without considering the free surface at  $h/d \geq 3.0$ , while that of frictional component is almost the same. When  $h/d \geq 3.0$ , the lateral force and yaw moment coefficients are almost the same as when the free surface is not considered. The error between the present numerical result and the measurements is within 10%, which indicates that RANS method has promising capability to predict the hydrodynamic forces on ships manoeuvring in shallow water.

## NOMENCLATURE

$B$	Breadth of ship (m)
$C_B$	Block coefficient
$C_{xf}$	Frictional components of drag coefficient
$C_{xp}$	Pressure components of drag coefficient
$C_x$	Coefficient of drag force
$C_{yf}$	Frictional components of lateral force coefficient
$C_{yp}$	Pressure components of lateral force coefficient
$C_y$	Coefficient of lateral force
$C_{nf}$	Frictional components of yaw moment coefficient
$C_{np}$	Pressure components of yaw moment coefficient
$C_n$	Coefficient of yaw moment
$d$	Draught (m)
$F_n$	Froude number
$F_x$	Drag (N)
$F_y$	Lateral force (N)
$h$	Water depth (m)
$L_{pp}$	Length between perpendiculars (m)
$M_z$	Yaw moment (N·m)
$R_e$	Reynolds number
$\rho$	Liquid density (kg/m <sup>3</sup> )
$\Delta$	Displacement (t)

## 1. INTRODUCTION

Assessment of ship manoeuvrability at the initial design stage is important from the aspect of safety and compliance with statutory regulations. The turning radius usually increases in shallow water condition, which will lead to deterioration of turning ability in shallow water (Hirano & Takashina, 2010). This is not always the case. In fact, high block vessels with twin screws can exhibit non-characteristic behaviours (e.g., the turning circles get small in shallow water). However, the hydrodynamic forces and moments acting on the ship need to be predicted.

The forces on the hull are determined either from towing tank experiments, semi-empirical formulas, numerical methods, or full-scale trial results. In the past time, the prediction of ship manoeuvrability relied more on captive model test and empirical formulas. Captive model tests such as planar motion mechanism and rotating arm tests are useful and reliable. However, they are expensive and time consuming. Similarly, the manoeuvring performances can also be predicted in the free running model tests. However, a large manoeuvring lake is required.

Additionally, these tests can be carried out only at model self-propulsion point, resulting in possible over prediction of manoeuvring performance. Numerical methods based on computational fluid dynamics (CFD) are cost effective. As the development of computer technology, the accuracy of results of simulation is getting better.

In order to estimate the hydrodynamic derivative of ships in shallow water area, Ohmori (1998) calculated the viscous flow around the ESSO OSAKA model using finite volume method in shallow water condition by considering the shallow bottom effect of the lateral additional mass of the transverse section of a two-dimensional hull. King *et al.* (2000) further improved the linear hydrodynamic derivative of ship navigating in the shallow water area, systematically expounded the interaction between ship hull and the bottom of the channel, and compared with the Mariner ship type test results, the linear velocity term and acceleration term of hydrodynamic derivative were consistent. Toxopeu *et al.* (2013) discussed the shallow water effect associated with the manoeuvring hydrodynamic force by comparing a wide range of CFD calculations with experimental data for KVLCC2. In this study, the effects of sidewalls and free surfaces were tested for correlation, and the hydrodynamic force owing to the restraint effect of hull motions such as sinkage and trim was compared. The analysis results for changes in the stern flow field were also shown very well. Yun *et al.* (2014) conducted a large-scale towing tank experiment with model ships of KCS and KVLCC2, and studied the hull squatting under shallow water conditions. As a result, with the increase of drift angle and the decrease of water depth, the squatting situation of the model ship changed significantly.

Jin *et al.* (2016) confirmed that the linear hydrodynamic derivative of swaying force was greatly affected by scale effect, while the yaw moment was less affected by scale effect. Xing *et al.* (2012) employed a hybrid RANS-LES model, the Detached Eddy Simulation (DES) in CFD for analysing fluid separations around the KVLCC2 hull at large drift angles. His research illustrated the formation of vortical and turbulent structures along the vessel in detail and confirmed their influences on the manoeuvring forces acting on the vessel. Dai and Miller and Atsavapranee *et al.* (2010) conducted steady turning simulations for a surface combatant 5617 with the RANS solver in CFD Ship-Iowa. Carrica (2016) studied the zigzag manoeuvring performance of KCS under shallow water conditions through experiments and CFD simulation, and obtained high-quality data suitable for CFD verification. In addition, grid research was also carried out to show the high CFD precision under self-propelled conditions. Wang (2009, 2012) carried out the numerical calculation of the viscous flow field of the hull in the deep water and shallow water respectively by using *SST k - ω* model. In order to evaluate the ship manoeuvrability in shallow water and deep water. He *et al.* (2016) used a RANS code for steering circle test and zigzag test, and obtained hydrodynamic

derivatives. The results show that the cycle of shallow water was larger than that of deep water, and the course-keeping performance of shallow water was improved. Dai and Miller (2011) examined the effects of actuator disk model on the overall fidelity of a RANS based ship manoeuvring simulations. Both experiments and simulations provided physical insights into the complex flow interactions between the hull and various appendages, the rudders, and the propellers. The simulations were compared with experimental results and they both demonstrated the cross-flow effect on the transverse forces and the propeller slip streams generated by the propellers during steady turning conditions.

Usually, the ship's manoeuvrability deteriorates as the water becomes shallower. In the present study, the hydrodynamic force of the ship in a certain water depth is numerically calculated and the numerical result is compared with measurements. And then, the effects of water depth and free-surface on the hydrodynamic forces of ship manoeuvring are obtained by calculating and analyzing the hydrodynamic forces of ship in different water depths with free-surface effect considered.

## 2. DESCRIPTION OF PROBLEM AND MATHEMATICAL MODEL

The physical problem of the fluid flow around a ship in steady turning motion can be described in the dual coordinate systems, as shown in Figure 1. The earth-fixed coordinate system is denoted by  $oXYZ$  and the ship-fixed coordinate system is denoted by  $o'xyz$ . The ship turns at a constant speed with a radius of  $R$  around the origin of the earth-fixed coordinate system. The  $R$  is twice the length of the ship.  $o'$  fixed to the ship is located at the intersection of middle ship section, middle plane and water surface.  $x$  axis points to the bow,  $y$  axis points to the starboard side,  $z$  axis perpendicular to the water surface is downward. The ship sails at three angular velocities  $\omega = 0.051, 0.072$  and  $0.109$ , corresponding to the Froude number  $F_n = 0.064, 0.09$  and  $0.136$  and

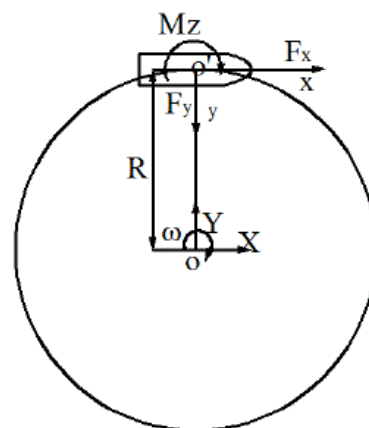


Figure 1. Coordinate system of a ship in steady turning motion

the Reynolds number  $Re = 1.49 \times 10^6$ ,  $2.1 \times 10^6$  and  $3.2 \times 10^6$  respectively.  $F_x$  and  $F_y$  are the components of hydrodynamic forces on the hull along the positive  $x$ -axis and along the positive  $y$ -axis respectively.  $M_z$  is the turning moment on the hull around the  $z$ -axis.

A large number of manoeuvring model tests have been carried out for the ESSO OSAKA oil tanker and a large amount of experimental data is available for validation of numerical method, so it is taken as an example in the present investigation. Numerical simulation is performed in model-fixed condition. The geometric model of the hull is shown in Figure 2. The principal dimensions of the ship and model are listed in Table 1.

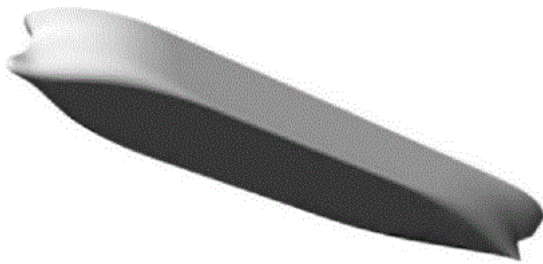


Figure 2. Geometry of the ESSO OSAKA Model

Table 1: Principal dimensions of ship and model

Designation	Full scale	Model scale
Length between perpendiculars $L_{pp}$ (m)	325	3.824
Breadth of ship $B$ (m)	53	0.624
Draught $d$ (m)	21.8	0.256
Displacement $\Delta$ (t)	314180	0.4986
Block coefficient $C_b$	0.831	0.831

When the governing equations are solved in a rotating frame of reference, the acceleration of the fluid appears as an additional term in the momentum equations. In the present study, computations are performed with the RANS solver of the CFD platform STAR-CCM+. The solver allows to use absolute velocity  $\vec{v}$  or relative velocity  $\vec{v}_r$  as independent variables to solve the problem of fluid flows. The relationship between the two velocities is:

$$\vec{v}_r = \vec{v} - (\vec{\omega} \times \vec{r}) \quad (1)$$

where  $\vec{r}$  is any position vector in a rotating frame of reference.

In the inertial system, the momentum equation is:

$$\frac{\partial}{\partial x}(\rho \vec{v}) + \nabla \cdot (\rho \vec{v} \vec{v}) = -\nabla p + \nabla \cdot \bar{\bar{\tau}} + \vec{F} \quad (2)$$

where  $\vec{F}$  is external volume force, and  $\bar{\bar{\tau}}$  is the viscous stress tensor.

$$\bar{\bar{\tau}} = \mu \left[ (\nabla \vec{v} + \nabla \vec{v}^T) - \frac{2}{3} \nabla \cdot \vec{v} I \right] \quad (3)$$

where  $I$  is the unit tensor. The momentum equations expressed in absolute velocity in the rotation reference frame are as follows:

$$\frac{\partial}{\partial x}(\rho \vec{v}) + \nabla \cdot (\rho \vec{v} \vec{v}) + \rho (\vec{\omega} \times \vec{v}) = -\nabla p + \nabla \cdot \bar{\bar{\tau}}_r + \vec{F} \quad (4)$$

The momentum equations are expressed with relative velocity in the rotation frame, as follows:

$$\begin{aligned} \frac{\partial}{\partial x}(\rho \vec{v}_r) + \nabla \cdot (\rho \vec{v}_r \vec{v}_r) + \rho (2\vec{\omega} \times \vec{v}_r + \vec{\omega} \times \vec{\omega} \times \vec{r}) + \\ \rho \frac{\partial \vec{\omega}}{\partial t} \times \vec{r} = -\nabla p + \nabla \cdot \bar{\bar{\tau}}_r + \vec{F} \end{aligned} \quad (5)$$

The momentum equations contain two additional acceleration terms in Eq. 5, as follows:

- (a) Coriolis acceleration:  $2\vec{\omega} \times \vec{v}_r$ ;
- (b) Centripetal acceleration:  $\vec{\omega} \times \vec{\omega} \times \vec{r}$ .

where  $\bar{\bar{\tau}}_r$  is the viscous stress tensor, and its calculation formula is:

$$\bar{\bar{\tau}}_r = \mu \left[ (\nabla \vec{v}_r + \nabla \vec{v}_r^T) - \frac{2}{3} \nabla \cdot \vec{v}_r I \right] \quad (6)$$

In a rotating frame of reference, the continuity equation takes the form of either absolute or relative velocity:

$$\frac{\partial u_i}{\partial x_i} = 0 \quad (7)$$

The transport equations for the SST  $k - \omega$  model (Menter, F. R, 1994) are:

$$\begin{aligned} \frac{\partial(\rho \omega)}{\partial t} + \text{div}(\rho \omega U) = \text{div} \left[ \left( \mu + \frac{\mu_t}{\sigma_{\omega,1}} \right) \text{grad}(\omega) \right] + \\ \gamma_2 \left( 2\rho S_{ij} \cdot S_{ij} - \frac{2}{3} \rho \omega \frac{\partial U_i}{\partial x_j} \delta_{ij} \right) - \beta_2 \rho \omega^2 \\ + 2 \frac{\rho}{\sigma_{\omega,2} \omega} \frac{\partial k}{\partial x_k} \frac{\partial \omega}{\partial x_k} \end{aligned} \quad (8)$$

The SST  $k - \omega$  turbulence model based on experience with the model in general-purpose computation:

$$\begin{aligned} \sigma_k = 1.0, \sigma_{\omega,1} = 2.0, \sigma_{\omega,2} = 1.17, \\ \gamma_2 = 0.44, \beta_2 = 2.0 \end{aligned} \quad (9)$$

### 3. NUMERICAL METHODS

#### 3.1 COMPUTATIONAL DOMAIN AND BOUNDARY CONDITIONS

For CFD simulation, the calculation accuracy is highly dependent on computational domain, wall treatment and grid number. In order to accurately solve the flow field around the vessel in turning motion, a cuboid computational domain is selected, as shown in Figure 3. Velocity inlet is set on the boundaries of front, left, right and top of the computational domain. No-slip wall condition is set on bottom boundary, and pressure outlet is set on the aft boundary. The range of the computational domain is  $-5.5L < x < 3.1L$ ,  $-1.3L < y < 5.3L$ , as to the position of  $z$ ,  $z < 0.3L$  is set above the water, the  $z$ -coordinate setting below the water surface is adjusted by the water depth (Berth, 1998). According to Permanent International Association of Navigation Congresses (PIANC) (1992),  $h/d > 3.0$  refers to deep water,  $1.5 < h/d < 3.0$  is medium deep water,  $1.2 < h/d < 1.5$  is shallow water, and  $h/d < 1.2$  is extremely shallow water. On this basis, the difference between deep water and shallow water is defined.

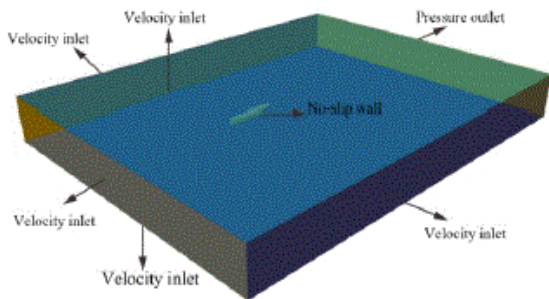


Figure 3. Computational domain and boundary conditions

#### 3.2 GRIDS GENERATION

The computational domain is discretized by using unstructured hexahedral cells. Meanwhile, finer grids around water surface are used to capture the features of free surface, as shown in Figure 4. The grids near bow and stern are also shown in this figure. The prismatic layer cells generated on the hull surface can resolve the near-wall flows. The prismatic layer parameters are set according to  $y^+$ . Wall  $y^+$  near hull surface is shown in Table 2.

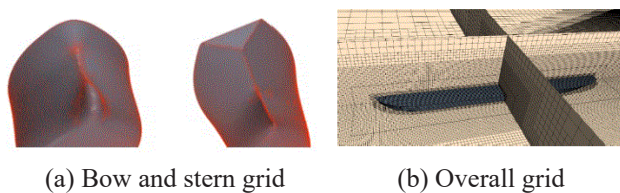


Figure 4. Computational meshes

Table 2: Wall  $y^+$  near hull surface.

Case	Cell Number	Wall $y^+$		
		Max	Min	Average
Coarse	2332438	42.6	0.59	15.18
Medium	5321242	15.3	0.14	4.31
Fine	11241400	4.59	0.019	0.75

The governing equations are discretized by the finite volume method (FVM). *SST*  $k - \omega$  turbulence model, which is more suitable for simulation of flow field around ship in turning motion than others (Wang, 2009), is used to enclose the governing equations. Accordingly, all  $y^+$  treatment is selected for near-wall modelling, which is a hybrid treatment employing wall function for coarse meshes and resolving viscous sub-layer for fine meshes. A two-phase volume of fluid (VOF) technique is used to capture the free surface.

The relative movement between earth-fixed and ship-fixed coordinate systems are applied to describe the ship motion. The desired motions are implemented in the earth-fixed coordinate system by moving the rotation of reference, instead of turning the whole computational domain. When rotating the reference, bottom boundary is set to be still. The time step is set to be 0.01s, and maximum inner iterations times is limited to 8.

### 4. VALIDATION OF NUMERICAL METHOD

#### 4.1 GRID DEPENDENCE STUDY

Before embarking upon the studying on the effects of the hydrodynamic forces acting on the turning ship, a critical assessment on the capacity of the proposed method is essential. The validation data used here are obtained from the rotating arm tank test (Berth, 1998), which was conducted in a rotating arm tank (65m radius  $\times$  5m depth).

In the grid spacing convergence study, all grid points are given as a percentage of the base size, which are changed systematically with a constant ratio to obtain grids of different density. Three sets of grids refer to as coarse ( $2.3 \times 10^6$ ), medium ( $5.3 \times 10^6$ ), and fine ( $11.2 \times 10^6$ ) are generated based on the refinement ratio of  $\sqrt{2}$ . The size of prismatic layer type cell and other regular grids for the three sets of meshes are increased with the increasing density.

Table 3 shows the coefficients of drag, lateral force and yaw moment calculated with the three sets of grids.

$$C_x = \frac{F_x}{\frac{1}{2} \rho U^2 \cdot L_{pp}^2} \quad (10)$$

Table 3: Grid convergence of forces on different grid

Grid case	Grid number ( $\times 10^6$ )	$C_x$	E%D	$C_y$	E%D	$C_n$	E%D
Coarse	2.3	-0.00114		0.00211		-0.00177	
Medium	5.3	-0.00119	5.79	0.00206	2.42	-0.00175	2.31
Fine	11.2	-0.00121	1.66	0.00208	0.96	-0.00173	1.15

$$C_y = \frac{F_y}{\frac{1}{2} \rho U^2 \cdot L_{pp}^2} \quad (11)$$

$$C_n = \frac{M_z}{\frac{1}{2} \rho U^2 \cdot L_{pp}^3} \quad (12)$$

The relative error of the numerical results is defined as  $E\%D = (S - D)/D \times 100$ , where D is the result by the fine meshes and S is that by the coarse or medium meshes respectively. The force coefficients by the medium and fine grids are almost same, especially for coefficient of lateral forces with the errors under the order 1%. The minor increase accuracy resulting from adding so many cells is not worthwhile. At the same time, to guarantee adequate precision and high efficiency in the numerical simulation, the method of medium grids generation is selected to perform the following simulations. The maximum cell size in the computational domain is 1cm. Figure 5 clearly shows the detailed free surface features captured in the case  $h/d = 10$ ,  $F_n = 0.136$ .

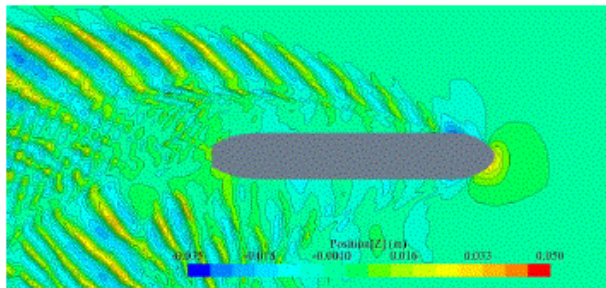


Figure 5. Contours of wave elevation

#### 4.2 VALIDATION

Calculated coefficients of drag, lateral force and yaw moment and the corresponding experimental ones in the case  $h/d = 10$ ,  $F_n = 0.136$ . (Berth, 1998) are compared in Table 4. It was seen that a good agreement is obtained. Errors of the calculated results are all within 10% relative to the experimental ones. Therefore, the present numerical method is valid for simulation of the flow around the ship undertaking steady turning motion.

Table 4: Comparison between present numerical results and measurements.

	CFD	EFD	Error (%)
$C_x$	$-1.21 \times 10^{-3}$	$-1.318 \times 10^{-3}$	-8.2%
$C_y$	$2.08 \times 10^{-3}$	$2.244 \times 10^{-3}$	-7.32%
$C_n$	$-1.73 \times 10^{-3}$	$-1.777 \times 10^{-3}$	2.64%

### 5. NUMERICAL RESULTS AND DISCUSSION

The effects of water depth on manoeuvring hydrodynamic forces acting on ship in steady turning motion are studied. For different water depths of  $h/d = 10.0, 5.0, 3.0, 2.0, 1.5$ , there are three different rotational speeds for hydrodynamic calculation, as shown in Table 4 ( $U_m = R \times \omega$ ,  $F_n$  is the Froude number).

$$F_n = \frac{U_m}{\sqrt{gL_{pp}}} \quad (13)$$

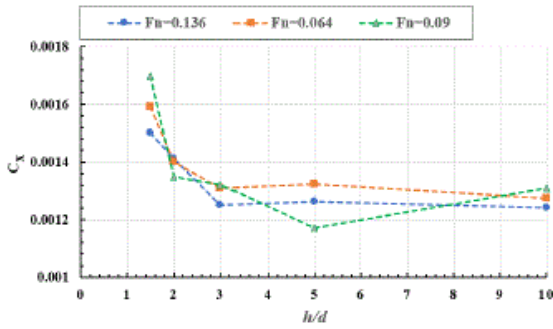
Where g is the acceleration of gravity.

Table 4. The Froude number for each turning speed

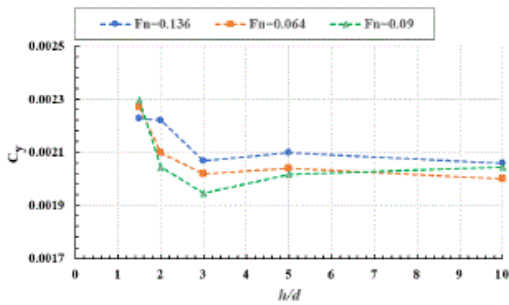
	$\omega$ (rad/s)	$U_m$ (m/s)	$F_n$
Case 1	0.051	0.39	0.064
Case 2	0.072	0.55	0.09
Case 3	0.109	0.836	0.136

#### 5.1 VISCOUS HYDRODYNAMIC FORCES

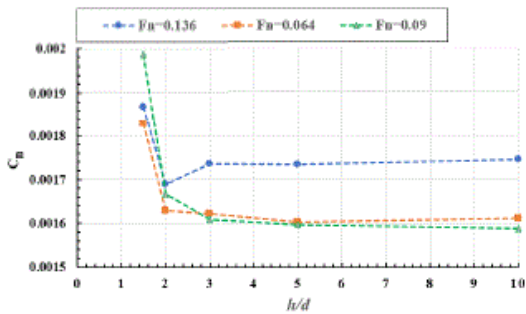
As shown in Figure 6, because of the Froude number being smaller than 0.15, the velocity effect is essentially dominated by viscosity which is expected to be small because of the relative narrowness of the Reynolds number range. In Figure 6(a), it was found that the drag coefficient hardly changes in the case of  $h/d \geq 3.0$ , especially for  $F_n = 0.064, 0.136$ . While it increases with water depth decrease when  $h/d \leq 3.0$ , and it increase dramatically when  $h/d \leq 2.0$ . There is not much difference between drag coefficients at different speeds except for that at  $h/d = 5$ , where the drag coefficient of  $F_n = 0.064$  is about 13% larger than that of  $F_n = 0.09$ .



(a) Drag coefficients



(b) Coefficients of lateral force



(c) Coefficients of yaw moments

Figure 6. Variation of hydrodynamic forces with water depth at different speeds

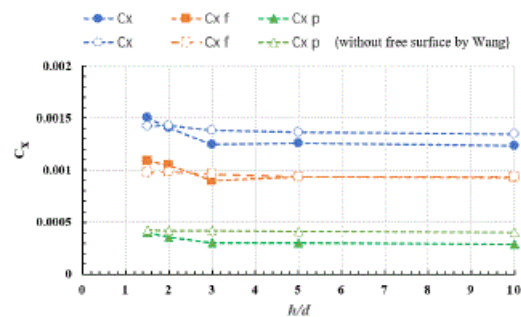
From Figure 6(b), it was found that, the trends of all three curves are almost the same, except for the case of  $F_n = 0.136$ . The coefficients of lateral force decrease a little from  $h/d = 5.0$  to  $h/d = 3.0$ , which might be because of the effect of free-surface leading to different wave elevation on the starboard and port sides of the hull, and they begin to increase rapidly with water depth decreasing in the case of  $h/d \leq 3.0$ . While it increases a little from  $h/d = 2.0$  to  $h/d = 1.5$  for  $F_n = 0.136$ . For both the case of  $h/d = 2.0$  and  $h/d = 3.0$ , the coefficients of lateral force at  $F_n = 0.136$  are about 10% larger than those at  $F_n = 0.09$ . While for the case of  $h/d = 1.5$ , the coefficient of lateral force at  $F_n = 0.136$  is about 3% smaller than that of  $F_n = 0.09$ .

In Figure 6(c), the coefficients of yaw moment at  $F_n = 0.064, 0.09, 0.136$  are almost unchanged from  $h/d = 3.0$  to  $h/d = 10.0$ . They are almost identical for  $F_n = 0.064, 0.09$ .

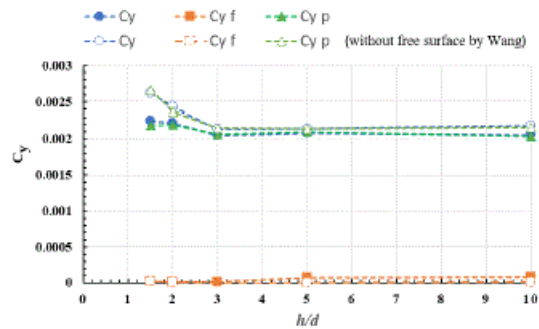
While the coefficients for  $F_n = 0.136$  are about 10% larger than those at the other two speed from  $h/d = 3.0$  to  $h/d = 10.0$ . The coefficients of yaw moment are almost the same at  $h/d = 2.0$ , while they increase rapidly with the water depth decrease when  $h/d \leq 2.0$ .

The coefficients of forces in the  $x$ - and  $y$ -directions and yaw moment are shown in Figure 7.  $C_{xp}$ ,  $C_{yf}$  and  $C_{nf}$  are the frictional components of the total forces and moment respectively, while  $C_{xp}$ ,  $C_{yp}$  and  $C_{np}$  are the pressure components.

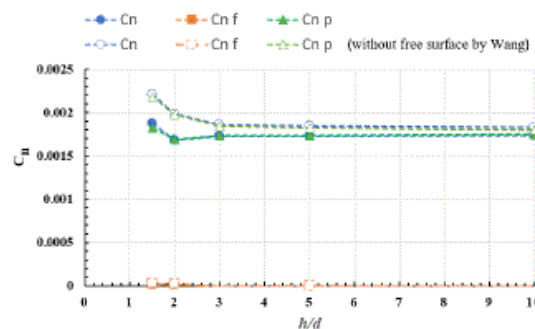
The three hydrodynamic coefficients all increase with the decrease of water depth. It was seen from Figure 7(a) that the effect of shallow water on the frictional components of drag coefficient is almost the same as that on pressure components of drag coefficient. Figure 7(b) and Figure 7(c)



(a) Drag coefficients



(b) Coefficients of lateral force



(c) Coefficients of yaw moments

Figure 7. Variation of the coefficients with water depth

show that the total lateral force and the yaw moment are mainly contributed by the pressure contribution regardless of the water depth, and the contribution of frictional is very small and might be ignored. The other CFD results are supplied by Wang (2009), which is carried by CFD solver FLUENT without considering the effect of free surface. Both coefficient of pressure component of drag force and drag coefficient in the present simulation are about 7% smaller than those by Wang at  $h/d \geq 3.0$ , while that of frictional component is at the same level with Wang's. The coefficients of lateral force and yaw moment are almost the same as those by Wang's at  $h/d \geq 3.0$ . Both  $C_y$  and  $C_{yp}$  are smaller than Wang's results about 20% at  $h/d = 1.5$ , and the case of yaw moment coefficient is similar to that of the lateral force coefficient.

### 5.2 VORTICITY DISTRIBUTION

The vorticity distributions on the sectional plane near the stern ( $x/L = -0.4$ ) are clearly shown in Figure 8. It was seen that, the range of vorticity on the port side region decreases with the decrease of water depth, while the distribution of vorticity on the starboard region does not change apparently with the water depth.

### 5.3 PRESSURE DISTRIBUTION ON THE HULL

Figure 10 shows the pressure distributions on the hull surface at different water depths. The left-hand column

shows the pressure on port side at  $F_n = 0.136$ , the right-hand column shows that on starboard side. The pressure value is dynamic pressure. It is observed that the pressure on surface near bow and stern is very high and does not change apparently with the water depth. While the lowest pressure distributed on the region near shoulder of the hull, and it is decreases obviously with water depth decreasing. This might cause the lateral force increase with water depth decreasing. The pressures on the hull surface near mid-ship on both sides become lower with water depth decreasing, while the pressure on the port side is higher than that on the star-board side at different water depths.

### 5.4 WAVE ELEVATION

Figure 9 shows the wave elevation on both sides of the hull. It was seen from Figure 9(a) that the wave elevation on the hull surface of starboard side near stern at  $h/d = 1.5$  are slightly higher than those at  $h/d = 2.0, 3.0$ . The wave elevations on the hull surface in the mid-ship region at  $h/d = 1.5$  and  $h/d = 3.0$  are very close, and that at  $h/d = 2.0$  is lower than them. On the surface near the bow, it was seen that wave elevation becomes higher as the water depth decreases. As shown in Figure 9(b), the wave elevation on the hull surface of port side near stern is very close to that of starboard side. While the wave elevation on the hull surface in the mid-ship region at  $h/d = 1.5$  is much higher than those at  $h/d = 2.0, 3.0$ . The wave elevations at the bow are nearly the same at all three water depths.

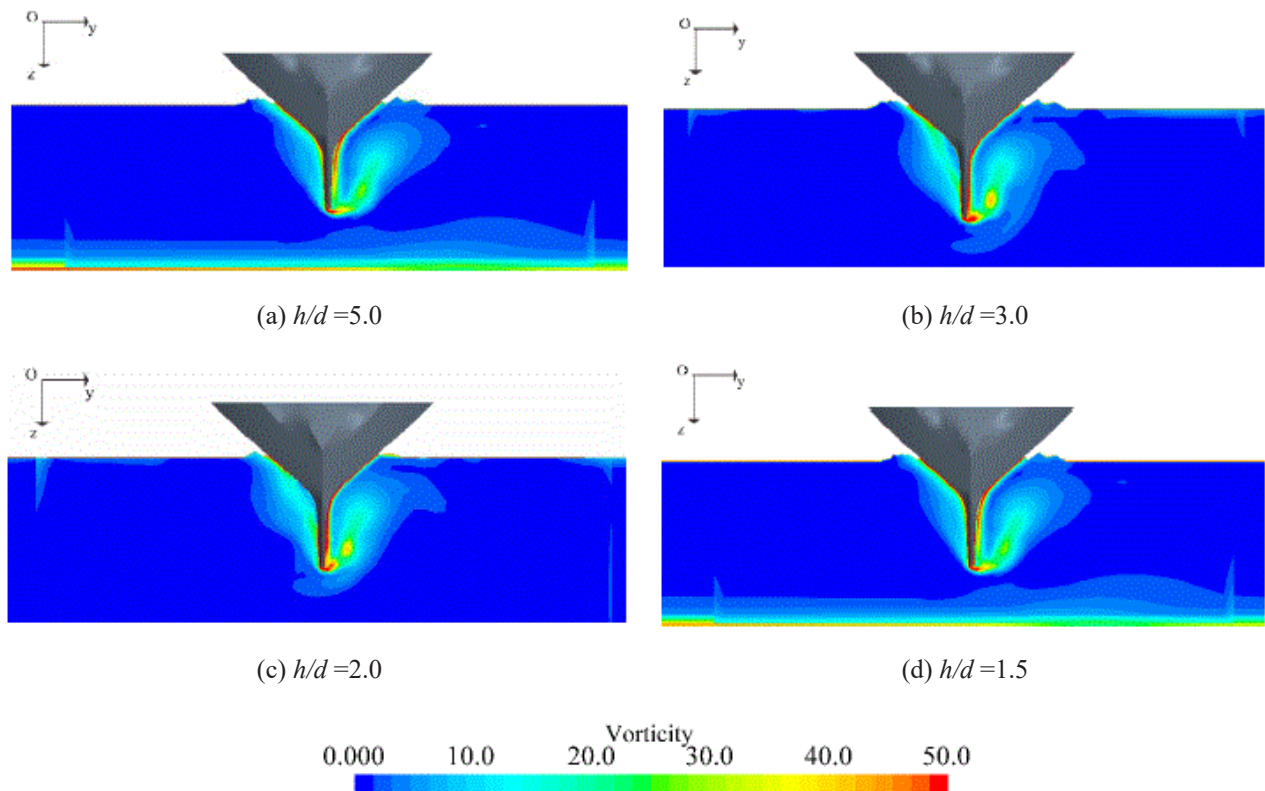
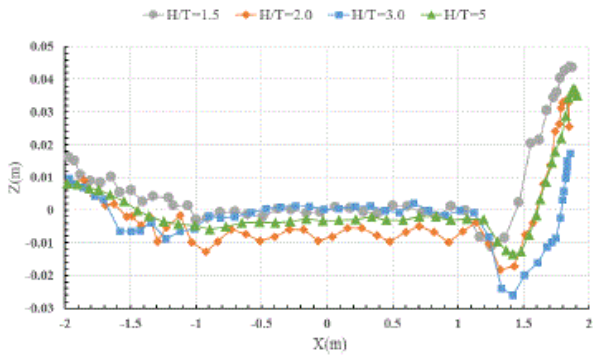
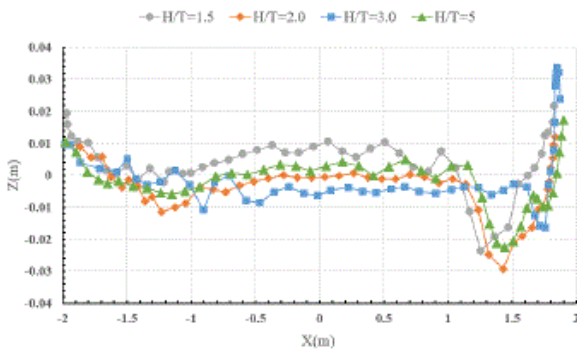


Figure 8. Vorticity distributions on the sectional plane at different water depths



(a) Wave elevation on starboard



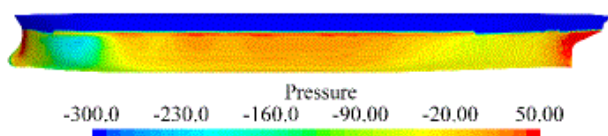
(b) Wave elevation on port

Figure 9. Wave elevation on hull surface

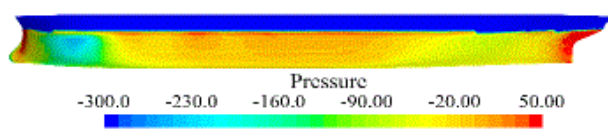
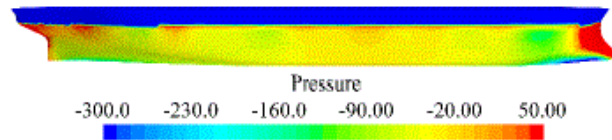
## 6. CONCLUSIONS

In the present study, the CFD method is used to investigate the hydrodynamic characteristics of the ESSO OSAKA model in deep and shallow waters, which performs steady turning motion with the effect of free surface considered. It was found that the hydrodynamic coefficients at different speeds are basically the same. The drag coefficient, lateral force coefficient and yaw moment coefficient of the ship in different water depths and different speeds are predicted, and the numerical results are compared with the experimental results. The results show that the hydrodynamic coefficients at different speeds are basically the same, and different water depths have a great influence on the hydrodynamic coefficients.

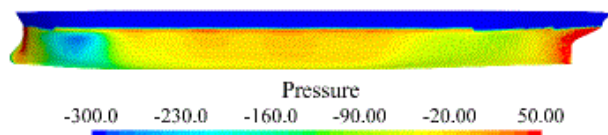
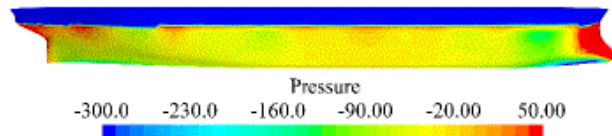
The present numerical results are in good agreement with the previously published measurements, which shows that CFD method is effective to predict the manoeuvring hydrodynamics of the ship in turning motion by solving RANS equations. From the numerical results, the lateral force and yaw moment become larger as the water depth becomes shallower, indicating that the ship's turning manoeuvre becomes more difficult. It is helpful to evaluate ship manoeuvrability in shallow water and has theoretical guiding significance for the safe manoeuvring of ships in shallow water.



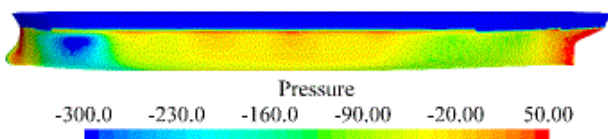
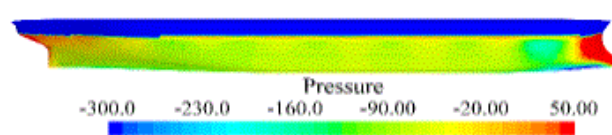
(a)  $h/d = 5.0$



(b)  $h/d = 3.0$



(c)  $h/d = 2.0$



(d)  $h/d = 1.5$

Figure 10. Pressure distribution on hull surface

1. At different water depths, the effects of speed on coefficients of drag, lateral force and yaw moment are small, and the difference between manoeuvring hydrodynamic coefficients at different speeds is within 10%.
2. The effect of water depth on the drag coefficient is significant. The three hydrodynamic coefficients all increase with the decrease of water depth. The drag coefficient at  $F_n = 0.09$  in shallow water ( $h/d = 1.5$ ) is about 45% larger than that in deep water ( $h/d = 5$ ). However, it has smaller effect on the lateral force coefficient, which is about 15% larger in shallow water than in deep water. While, it has great effect on the yaw moment coefficient, which is about 25% larger in shallow water than in deep water.
3. The effects of free surface on coefficients of lateral force and yaw moment are greater than on drag coefficient. The present coefficients of the lateral force and yaw moment at  $F_n = 0.136$  &  $h/d = 1.5$  with effect of free surface considered are about 20% smaller than those without effect of free surface considered. The coefficients of lateral force decrease a little from  $h/d = 5.0$  to  $h/d = 3.0$ . It can be found that the effect of the free surface is significant on the manoeuvrability of ship in turning motion in shallow water.

## 7. ACKNOWLEDGEMENTS

This work is supported by the National Natural Science Foundation of China (No.51809236), Zhejiang Province Key Research and Development Project (No. 2021C02184) and the Open Foundation from Key Laboratory of Offshore Engineering Technology of Zhejiang.

## 8. REFERENCES

1. ATSAVAPRANEE, P.; MILLER, R.; DAI, C., *et al.* (2010) *Steady-turning experiments and RANS simulations on a surface combatant hull form (Model#5617)*, in: Proceedings of 28th Symposium on Naval Hydrodynamics. Pasadena.
2. BERTH, F.; BIGOT E. and LAURENS, J. M. (1998) *Numerical simulation on the ESSO OSAKA*, in: Proceedings of MAN'98. Val de Reuil, France, pp. 109–116. Val de Reuil, France.
3. CARRICA, P. M.; MOFIDI, A.; ELOOT, K., *et al.* (2016) *Direct simulation and experimental study of zigzag maneuver of KCS in shallow water*. Ocean Eng. 112, pp. 117–133.
4. DAI, C. M. and MILLER, R. W. (2011) *URANS simulation of an appended hull during steady turn with propeller represented by an actuator disk model*, in: Proceedings of ASME International Conference on Ocean. Rotterdam. The Netherlands.
5. HIRANO, M. and TAKASHINA, J. (2010) *Ship manoeuvrability: theory and its application*. Mitsui Akishima Research Laboratory, Japan.
6. HE, S.; KELLETT, P.; YUAN, Z., *et al.* (2016) *Manoeuvring prediction based on CFD generated derivatives*. J. Hydrodyn. 28(2), pp. 284–292.
7. JIN, Y.; DUFFY, J.; CHAI, S., *et al.* (2016). *URANS study of scale effects on hydrodynamic maneuvering coefficients of KVLCC2*. Ocean. Eng. 118, pp. 93–106.
8. KING, D. J.; BAKOUNTOUZIS, L. and KATORY, M. (2000) *Predicting of ship hydrodynamic derivatives in shallow and restricted waters*. J. International Shipbuilding progress. 47(452), pp. 379–396.
9. MENTER, F. R. (1994) *Two-equation eddy-viscosity turbulence models for engineering applications*. J. AIAA, 32(8), pp. 1598–1605.
10. OHMORI, T. (1998) *A study on hydrodynamic characteristics of a maneuvering ship in shallow water by a finite-volume method*, in: Proceedings of the MAN'98 International Symposium and Workshop on Force Acting on a Maneuvering Vessel. Bassin d'Essais des Carenes, Val de Reuil, France.
11. Permanent International Association of Navigation Congresses (PIANC) (1992) *Capability of ship maneuvering simulation models for approach channels and fairways in harbours*, in: Report of Working Group no. 20 of Permanent Technical Committee II. Supplement to PIANC Bulletin No. 77, Brussels.
12. SAKAMOTO, N.; CARRICA, P. M. and STERN, F. (2011) *URANS simulations of static and dynamic maneuvering for surface combatant: part 1. verification and validation for forces, moment, and hydrodynamic derivatives*. J. Mar. Sci. Technol. 17(4), pp. 422–445.
13. SAKAMOTO, N.; CARRICA, P. M. and STERN, F. (2012) *URANS simulations of static and dynamic maneuvering for surface combatant: part 2. verification and validation for forces, moment, and hydrodynamic derivatives*. J. Mar. Sci. Technol. 17(4), pp. 446–468.
14. TOXOPEUS, S. L.; SIMONSEN, C. D.; GUILMINEAU, E., *et al.* (2013) *Investigation of water depth and basin wall effects on KVLCC2 in manoeuvring motion using viscous-flow calculations*. J. Mar. Sci. Technol. 18, pp. 471–496.
15. WANG, H. M. (2009) *Numerical study on the viscous flow and hydrodynamic forces on a manoeuvring ship in restricted waters*. Doctoral esis, Shanghai Jiao Tong University, Shanghai, China.
16. WANG, H. M. (2012) *Numerical study on hydrodynamic performance of submarine in turning motion*, in: Proceedings of The International Workshop on Next Generation of Nautical Traffic Model. Shanghai, China.

17. XING, T.; BHUSHAN, S. and STERN, F. (2012) *Vortical and turbulent structures for KVLCC2 at drift angle 0, 12, and 30°*. Ocean Eng. 55, pp. 23–43.
18. YUN, K. H.; PARK, B. J. and YEO, D. J. (2014) *Experimental study of ship squat for KCS in shallow water*. J. Soc. Nav. Archit. Korea 51(1), pp. 34–41.
19. YUN, K. H.; PARK, K. R. and PARK, B. J. (2014) *Study of ship squat for KVLCC2 in shallow water*. J. Soc. Nav. Archit. Korea 51(6), pp. 539–547.